Received: 28 June 2023 | Revised: 6 July 2023 | Accepted: 22 August 2023

DOI: 10.1002/pamm.202300062

RESEARCH ARTICLE

Efficient Newton-multigrid FEM solver for multifield nonlinear coupled problems applied to thixoviscoplastic flows

Naheed Begum | **Abderrahim Ouazzi** | **Stefan Turek**

Institute for Applied Mathematics, LSIII, TU Dortmund University, Dortmund, Germany

Correspondence
Naheed Begum, Institute for Applied Mathematics, LSIII, TU Dortmund University, D-44227 Dortmund, Germany.
Email: Naheed.Begum@math.tu-dortmund.de

Funding information
Deutsche Forschungsgemeinschaft, Grant/Award Number: 446888252

Abstract

This note is concerned with efficient Newton-multigrid finite element method (FEM) solver for multifield nonlinear flow problems. In our approach, for efficient FEM solver, we advantageously use the delicate symbiosis aspects of the problem settings for FEM approximations, and the algorithmic tools to obtain the numerical solutions. We concretize our ideas on thixoviscoplastic flow problems. It is a two-field coupled nonlinear problem. And beside the integrated nonlinearity within momentum and microstructure equations, thixoviscoplastic problems induce a nonlinear two-way coupling. As far as FEM numerical solutions are concerned, we set the problem in a suitable variational form to use the corresponding wellposedness analysis to develop FEM techniques for the solver. Indeed, the wellposedness study is not an intellectual exercise, rather it is the foundation for the approximate thixoviscoplastic problem as well as for the development of an efficient solver. We base our investigations for the solver on our wellposedness and error analysis results of thixoviscoplastic flow problems published in *Proc. Appl. Math. Mech*. We continue our series, and proceed to develop a monolithic Newton-multigrid thixoviscoplastic solver. The solver is based on Newton's method and geometric multigrid techniques to treat the coupling of the problem. So, we use Local Pressure Schur Complement (LPSC) concept to solve the coupled problem on mesh's elements, and proceed with outer blocks Gauss-Seidel iteration to update the global solutions. Furthermore, we handle the nonlinearity of the problem with the combined adaptive discrete Newton's and multigrid methods. The adaptivity within discrete Newton's method is based on the adaptive step-length control for the discrete differencing in the Jacobian calculations, while the convergence of linear multigrid solver is made to match the convergence requirement of nonlinear solver, accordingly. And the solver's update parameters are solely dependent on the actual convergence rate of the nonlinear problem. We provide the numerical results of solver performance for thixoviscoplastic lid-driven cavity flow.

This is an open access article under the terms of the Creative Commons Attribution-NonCommercial License, which permits use, distribution and reproduction in any medium, provided the original work is properly cited and is not used for commercial purposes.
© 2023 The Authors. *Proceedings in Applied Mathematics and Mechanics* published by Wiley-VCH GmbH.

KEYWORDS
efficient simulation techniques for CFD problems, filled polymer simulations, newton-multigrid methods, thixotropic flow problems, viscoplastic flow problems

1 | INTRODUCTION

We shall consider efficient finite element method (FEM) solver formultifield nonlinear saddle-point problem of the following system: *Find* $(\boldsymbol{u}, p, \lambda) \in \mathbb{V} \times \mathbb{Q} \times \mathbb{T}$ *such that*

$$\begin{cases} a_{\boldsymbol{u}}(\boldsymbol{u}, \lambda)(\boldsymbol{u}, \boldsymbol{v}) + b(\boldsymbol{v}, p) = l_{\boldsymbol{u}}(\boldsymbol{v}) & \forall\, \boldsymbol{v} \in \mathbb{V}, \\ b(\boldsymbol{u}, q) = 0 & \forall\, q \in \mathbb{Q}, \\ a_{\lambda}(\boldsymbol{u}, \lambda)(\lambda, \xi) = l_{\lambda}(\xi) & \forall\, \xi \in \mathbb{T}, \end{cases} \tag{1}$$

where, $a_{\boldsymbol{u}}$, b, and a_{λ} are bounded forms on $\mathbb{V} \times \mathbb{T} \times \mathbb{V} \times \mathbb{V}$, $\mathbb{V} \times \mathbb{Q}$, and $\mathbb{V} \times \mathbb{T} \times \mathbb{T} \times \mathbb{T}$, respectively, and where $l_{\boldsymbol{u}}$, and l_{λ} are bounded linear form defined on dual spaces $\mathbb{V}'$, and $\mathbb{T}'$, respectively. The problem (1) is coupled via $(\boldsymbol{u}, p)$ and $(\boldsymbol{u}, \lambda)$. The nonlinearity of the problem (1) is only with respect to the two-field $(\boldsymbol{u}, \lambda)$. The aim is to advantageously use the delicate symbiosis aspects of the problem settings for FEM approximations, and the algorithmic tools to develop efficient solver for the numerical solutions.

The problem (1) arises from the quasi-Newtonian modeling approach of Houška thixoviscoplstic model [3].

$$\begin{cases} \left(\frac{\partial}{\partial t} + u \cdot \nabla\right)\boldsymbol{u} - \boldsymbol{\nabla} \cdot \left(2\mu(D_{\mathrm{II},r}, \lambda)\mathbf{D}(\boldsymbol{u})\right) + \nabla p = \boldsymbol{f}_{\boldsymbol{u}}, \\ \nabla \cdot \boldsymbol{u} = 0, \\ \left(\frac{\partial}{\partial t} + u \cdot \nabla\right)\lambda - \mathcal{F}(D_{\mathrm{II}}, \lambda) + \mathcal{G}(D_{\mathrm{II}}, \lambda) = f_{\lambda}, \end{cases} \tag{2}$$

in Ω, with external forces $\boldsymbol{f}_{\boldsymbol{u}}$, and f_{λ}. $\boldsymbol{u}$, p, and λ denote velocity, pressure, and microstructure, respectively. Different thixortopic models can be integrated via the extended viscosity, $\mu(\cdot, \cdot)$, buildup $\mathcal{F}(\cdot, \cdot)$, and breakdown $\mathcal{F}(\cdot, \cdot)$ functions dependent on the shear rate via the regularization of Forbenius norm of symmetric part of velocity gradient, $D_{\mathrm{II},r}$, beside the microstructure, λ. Thixoviscoplastic flow equations (2) induce two-way coupling of viscoplastic flow equations, and microstructure equation. On one hand, the extended viscosity function integrates the microstructure via thixotropic plastic viscosity and thixotropic yield stress. On other hand, the microstructure evolution equation integrates nonlinear buildup and breakdown functions, dependent on shear rate and microstructure, responsible for the competition process of Aging and Rejunevation. We refer to Table A1 for detailed description of some prototype thixotropic models.

We set the spaces $\mathbb{V} := (H_0^1(\Omega))^2$, $\mathbb{Q} := L_0^2(\Omega)$, and $\mathbb{T} := H^1(\Omega)$, associated with the corresponding norms H^1-norm $\|\cdot\|_1$ and L^2-norm $\|\cdot\|_0$, respectively, $\mathbb{V}'$, $\mathbb{Q}'$, and $\mathbb{T}'$ their corresponding dual spaces, respectively [4]. And we introduce the strong operators $\mathcal{A}_{\boldsymbol{u}}, \mathcal{L}_{\boldsymbol{u}} : \mathbb{V} \times \mathbb{T} \times \mathbb{V} \longrightarrow \mathbb{V}'$, and $\mathcal{N}_{\boldsymbol{u}} : \mathbb{V} \times \mathbb{V} \longrightarrow \mathbb{V}'$ as follows

$$\langle \mathcal{L}_{\boldsymbol{u}}(\boldsymbol{u}, \lambda)\boldsymbol{u}, \boldsymbol{v}\rangle = \int_{\Omega} 2\mu(D_{\mathrm{II},r}, \lambda)\mathbf{D}(\boldsymbol{u}) : \mathbf{D}(\boldsymbol{v})\, dx \qquad \forall \boldsymbol{u}, \boldsymbol{v} \in \mathbb{V}, \lambda \in \mathbb{T}, \tag{3}$$

$$\langle \mathcal{N}_{\boldsymbol{u}}(\boldsymbol{w})\boldsymbol{u}, \boldsymbol{v}\rangle = \int_{\Omega} \boldsymbol{w} \cdot \nabla \boldsymbol{u}\, \boldsymbol{v}\, dx \qquad \forall \boldsymbol{u}, \boldsymbol{v}, \boldsymbol{w} \in \mathbb{V}, \tag{4}$$

and set

$$\mathcal{A}_{\boldsymbol{u}}(\boldsymbol{u}, \lambda) := \mathcal{N}_{\boldsymbol{u}}(\boldsymbol{u}) + \mathcal{L}_{\boldsymbol{u}}(\boldsymbol{u}, \lambda). \tag{5}$$

RIGHTSLINK

16177061, 2023, 2, Downloaded from https://onlinelibrary.wiley.com/doi/10.1002/pamm.202300062 by Technische Universitaet Dortmund Dezernat Finanzen und Beschaffung, Wiley Online Library on [24/10/2024]. See the Terms and Conditions (https://onlinelibrary.wiley.com/terms-and-conditions) on Wiley Online Library for rules of use; OA articles are governed by the applicable Creative Commons License

The following operators $\mathcal{A}_\lambda, \mathcal{M}_\lambda : \mathbb{V} \times \mathbb{T} \longrightarrow \mathbb{T}'$, and $\mathcal{N}_\lambda : \mathbb{V} \times \mathbb{T} \longrightarrow \mathbb{T}'$ as follows

$$\langle \mathcal{M}_\lambda(\boldsymbol{u}, \lambda), \xi \rangle = \int_\Omega \left(-\mathcal{F}(D_{\mathrm{II},r}, \lambda) + \mathcal{G}(D_{\mathrm{II},r}, \lambda) \right) \xi \, d\Omega \qquad \forall \lambda, \xi \in \mathbb{T}, \boldsymbol{u} \in \mathbb{V}, \tag{6}$$

$$\langle \mathcal{N}_\lambda(\boldsymbol{u})\lambda, \xi \rangle = \int_\Omega \boldsymbol{u} \cdot \nabla \lambda \, \xi \, dx \qquad \forall \lambda, \xi \in \mathbb{T}, \boldsymbol{u} \in \mathbb{V}, \tag{7}$$

and set

$$\mathcal{A}_\lambda(\boldsymbol{u}, \lambda) := \mathcal{N}_\lambda(\boldsymbol{u}) + \mathcal{M}_{\boldsymbol{u}}(\boldsymbol{u}, \lambda). \tag{8}$$

The following linear forms $\mathcal{B} : \mathbb{V} \longrightarrow \mathbb{Q}'$, $l_{\boldsymbol{u}} : \mathbb{V} \longrightarrow \mathbb{R}$, and $l_\lambda : \mathbb{T} \longrightarrow \mathbb{R}$ as follows

$$\langle \mathcal{B}\boldsymbol{u}, q \rangle = -\int_\Omega \nabla \boldsymbol{u} \, q \, dx \qquad \forall \boldsymbol{u} \in \mathbb{V}, q \in \mathbb{Q}, \tag{9}$$

$$l_{\boldsymbol{u}}(\boldsymbol{v}) = \int_\Omega \boldsymbol{f}_{\boldsymbol{u}} \boldsymbol{v} \, dx \qquad \forall \boldsymbol{v} \in \mathbb{V}, \tag{10}$$

$$l_\lambda(\xi) = \int_\Omega f_\lambda \, \xi \, dx \qquad \forall \xi \in \mathbb{T}, \tag{11}$$

The weak formulation for thixoviscoplastic flow problems (2) is described by the system (1) with the operators $a_{\boldsymbol{u}}(\boldsymbol{u}, \lambda)(\cdot, \cdot)$, $a_\lambda(\boldsymbol{u}, \lambda)(\cdot, \cdot)$, and $b(\cdot, \cdot)$, given as follows

$$a_{\boldsymbol{u}}(\boldsymbol{u}, \lambda)(\boldsymbol{u}, \boldsymbol{v}) = \langle \mathcal{A}_{\boldsymbol{u}}(\boldsymbol{u}, \lambda)\boldsymbol{u}, \boldsymbol{v} \rangle \qquad \forall \boldsymbol{u}, \boldsymbol{v} \in \mathbb{V}, \lambda \in \mathbb{T}, \tag{12}$$

$$a_\lambda(\boldsymbol{u}, \lambda)(\lambda, \xi) = \langle \mathcal{A}_\lambda(\boldsymbol{u}, \lambda)\lambda, \xi \rangle \qquad \forall \boldsymbol{u} \in \mathbb{V}, \lambda, \xi \in \mathbb{T}, \tag{13}$$

$$b(\boldsymbol{v}, q) = \langle \mathcal{B}\boldsymbol{v}, q \rangle \qquad \forall \boldsymbol{u}, \boldsymbol{v} \in \mathbb{V}, q \in \mathbb{Q}. \tag{14}$$

The corresponding results for existence and uniqueness of the solutions to the problems can be found in literature [1].

2 | FINITE ELEMENT DISCRETIZATION

Let the domain Ω be partitioned by a grid $\mathcal{T}_h$, which are assumed to be quadrilaterals. For an element $K \in \mathcal{T}_h$, we denote by $\mathcal{E}(K)$ the set of all one-dimensional edges of K, and by $\mathcal{E}_i$ the set of all interior element edges of the grid $\mathcal{T}_h$

$$\mathcal{E}_i := \bigcup_{k \in \mathcal{T}_h} \{E \in \mathcal{E}(K) \mid E \cap \partial\Omega = \emptyset\}. \tag{15}$$

We define the conforming finite element spaces $\mathbb{V}_h \subset \mathbb{V}$, $\mathbb{T}_h \subset \mathbb{T}$, and $\mathbb{Q}_h \subset \mathbb{Q}$ as follows:

$$\mathbb{V}_h = \left\{ \boldsymbol{v}_h \in \mathbb{V}, \boldsymbol{v}_{h|K} \in \ (Q_2(K))^2 \, \forall \, K \in \mathcal{T}_h, \ \boldsymbol{v}_h = 0 \text{ on } \partial\Omega_h \right\}, \tag{16}$$

$$\mathbb{T}_h = \left\{ \xi_h \in \mathbb{T}, \xi_{h|K} \in \ Q_2(K) \, \forall \, K \in \mathcal{T}_h \right\}, \tag{17}$$

$$\mathbb{Q}_h = \left\{ q_h \in \mathbb{Q}, q_{h|K} \in \ P_1^{\mathrm{disc}}(K) \, \forall \, K \in \mathcal{T}_h \right\}, \tag{18}$$

where Q_r and P_r are polynomials with maximum power in each coordinate less or equal r, and total power less or equal r, respectively. In what follows, the polynomial power r is set to equal 2. Figure 1 exposes the distribution of degrees of freedom for the flow fields.

RIGHTSLINK

16177061, 2023, 2, Downloaded from https://onlinelibrary.wiley.com/doi/10.1002/pamm.202300062 by Technische Universitaet Dortmund Dezernat Finanzen und Beschaffung, Wiley Online Library on [24/10/2024]. See the Terms and Conditions (https://onlinelibrary.wiley.com/terms-and-conditions) on Wiley Online Library for rules of use; OA articles are governed by the applicable Creative Commons License

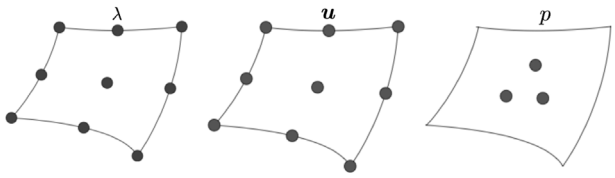

FIGURE 1 FEM pair for thixoviscoplastic flow problem: higher order FEM pair $Q_2/Q_2/P_1^{disc}$.

The approximated multifield nonlinear saddle-point problem of the following system:
Find $(\boldsymbol{u}_h, p_h, \lambda_h) \in \mathbb{V}_h \times \mathbb{Q}_h \times \mathbb{T}_h$ *such that*

$$\begin{cases} a_{\boldsymbol{u}}(\boldsymbol{u}_h, \lambda_h)(\boldsymbol{u}_h, \boldsymbol{v}_h) + b(\boldsymbol{v}_h, p_h) = l_{\boldsymbol{u}}(\boldsymbol{v}_h) & \forall\, \boldsymbol{v}_h \in \mathbb{V}_h, \\ b(\boldsymbol{u}_h, q_h) = 0 & \forall\, q_h \in \mathbb{Q}_h, \\ a_\lambda(\boldsymbol{u}_h, \lambda_h)(\lambda_h, \xi_h) = l_\lambda(\xi_h) & \forall\, \xi_h \in \mathbb{T}_h. \end{cases} \tag{19}$$

The details for the existence and uniqueness of the approximate thixoviscoplastic problem (19) and the best approximation can be found in literature[1]. The discrete matrix form of the approximate thixoviscoplastic problem supplemented with stabilization terms to enhance coercivity for the microstructure, and to stabilize the convection for velocity is given as follows

$$\begin{bmatrix} \mathbf{A}_{\boldsymbol{u}} + \mathbf{J}_{\boldsymbol{u}} & \mathbf{0} & \mathbf{B}^{\mathrm{T}} \\ \mathbf{0} & \mathbf{A}_\lambda + \mathbf{J}_\lambda & \mathbf{0} \\ \mathbf{B} & \mathbf{0} & \mathbf{0} \end{bmatrix} \begin{bmatrix} \boldsymbol{u} \\ \lambda \\ p \end{bmatrix} = \begin{bmatrix} Rhs_{\boldsymbol{u}} \\ Rhs_\lambda \\ Rhs_p \end{bmatrix} \tag{20}$$

The bilinear velocity and microstructure edge-oriented stabilizations $j_{\boldsymbol{u}}(\cdot,\cdot)$, and $j_\lambda(\cdot,\cdot)$ are defined as follows

$$j_{\boldsymbol{u}}(\boldsymbol{u}_h, \boldsymbol{v}_h) = \sum_{E \in \mathcal{E}_i} \gamma_{\boldsymbol{u}} |E|^2 \int_E [\nabla \boldsymbol{u}_h]\,[\nabla \boldsymbol{v}_h]\, d\sigma \qquad \forall\, \boldsymbol{u}_h, \boldsymbol{v}_h \in \mathbb{V}_h, \tag{21}$$

$$j_\lambda(\lambda_h, \xi_h) = \sum_{E \in \mathcal{E}_i} \gamma_\lambda |E|^2 \int_E [\nabla \lambda_h]\,[\nabla \xi_h]\, d\sigma \qquad \forall\, \lambda_h, \xi_h \in \mathbb{T}_h, \tag{22}$$

where $\gamma_{\boldsymbol{u}}$ and γ_λ are user-given parameters.

3 | MONOLITHIC NEWTON-MULTIGRID THIXOVISCOPLASTIC SOLVER

Let $\{\varphi_i, i = 1, 2, \ldots, \mathtt{dim}\mathbb{W}_h\}$ and $\{\psi_i,\ i = 1, 2, \ldots, \mathtt{dim}\mathbb{Q}_h\}$ denote the basis of the spaces $\mathbb{W}_h := \mathbb{V}_h \times \mathbb{T}_h$ and $\mathbb{Q}_h$, respectively. Thus, the vector solution $\mathcal{U} := (\boldsymbol{u}_h, \lambda_h, p_h) = (\tilde{\boldsymbol{u}}_h, p_h) \in \mathbb{W}_h \times \mathbb{Q}_h$ is expressed as

$$\mathcal{U} = \sum_{i=1}^{\mathtt{dim}\mathbb{W}_h} \tilde{\boldsymbol{u}}_i \varphi_i + \sum_{i=1}^{\mathtt{dim}\mathbb{Q}_h} p_i \psi_i \tag{23}$$

and the nonlinear discrete residuals for the system (20) is denoted as $\mathcal{R}(\mathcal{U}) \in \mathbb{R}^{\mathtt{dim}\mathbb{W}_h + \mathtt{dim}\mathbb{Q}_h}$

$$R(\mathcal{U}) = \big(\mathcal{R}_{\boldsymbol{u}}(\boldsymbol{u}_h, \lambda_h, p_h), \mathcal{R}_\lambda(\boldsymbol{u}_h, \lambda_h), \mathcal{R}_p(\boldsymbol{u}_h, p_h)\big) = \big(\mathcal{R}_{\tilde{\boldsymbol{u}}}(\tilde{\boldsymbol{u}}, p), \mathcal{R}_p(\tilde{\boldsymbol{u}}, p)\big) \tag{24}$$

We use adaptive discrete Newton to linearize the nonlinear discrete Residual (24). The Algorithm 1 shows the solver steps.

The step-length control parameter ε_l is adaptively dependent on the actual rate of residual convergence r_l [5, 6]. Furthermore, the damping parameter ω_l is set to unity.

In order to solve the linear systems, step (iv) in Algorithm 1, we use geometric multigrid solver. Thus, we set $\{\mathcal{T}_{h_k}\}$ to be a family of hierarchy multilevel triangulations associated with mesh size h_k, That is, we split each element on level trian-

RIGHTSLINK

16177061, 2023, 2, Downloaded from https://onlinelibrary.wiley.com/doi/10.1002/pamm.202300062 by Technische Universitaet Dortmund Dezernat Finanzen und Beschaffung, Wiley Online Library on [24/10/2024]. See the Terms and Conditions (https://onlinelibrary.wiley.com/terms-and-conditions) on Wiley Online Library for rules of use; OA articles are governed by the applicable Creative Commons License

ALGORITHM 1 Adaptive Newton via adaptive step-length control parameter

Result: $\mathcal{U}^{l+1} = \mathcal{U}^l - \omega_l \delta\mathcal{U}^l$, $\omega_l \in (0, 1]$
$r_0 = \left\|\mathcal{R}(\mathcal{U}^0)\right\|$, ε_0;
while $r_l \geq r_c$;
do
(i) **Calculate convergence rate** $r_l = \frac{\left\|\mathcal{R}(\mathcal{U}^l)\right\|}{\left\|\mathcal{R}(\mathcal{U}^{l-1})\right\|}$;
(ii) **Step-length size update** $\varepsilon_{l+1} = g(r_l)\varepsilon_l$;
(iii) **Calculate FD Jacobian** $\left[\mathcal{J}(\mathcal{U}^l)\right]_{ij} \approx \frac{\left(\mathcal{R}_i(\mathcal{U}^l + \varepsilon_l \boldsymbol{e}_j) - \mathcal{R}_i(\mathcal{U}^l - \varepsilon_l \boldsymbol{e}_j)\right)}{2\varepsilon_l}$;
(iv) **Solve via GMG** $\mathcal{J}(\mathcal{U}^l)\delta\mathcal{U}^l = \mathcal{R}(\mathcal{U}^l)$;
end

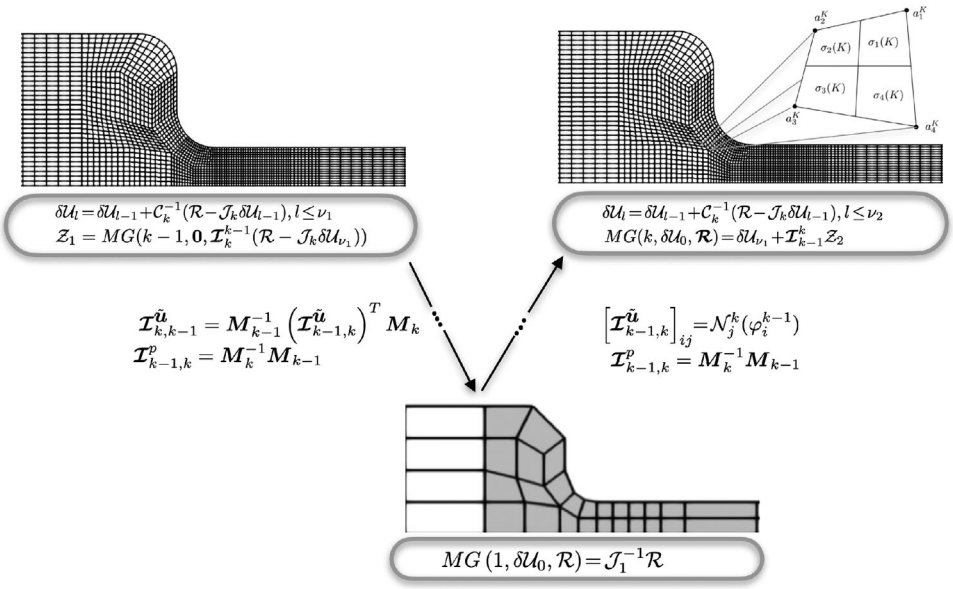

FIGURE 2 Coupled Geometric-MG solver: two-grid Algorithm on a prototype mesh-slice.

gulations $\mathcal{T}_{h_{k-1}}$ into 2^d $(d = 2)$ new sub-elements to get level triangulations $\mathcal{T}_{h_k}$ denoted by $\sigma_i(K)$, $i = 1, \ldots, 2^d$ (Figure 2). We set $\mathcal{W}_k := \mathbb{R}^{\dim\mathbb{W}_{h_k}}$, $\mathcal{Q}_k := \mathbb{R}^{\dim\mathbb{Q}_{h_k}}$, $\mathcal{V}_k := \mathcal{W}_k \times \mathcal{Q}_k$ and let $\boldsymbol{\mathcal{I}}_k^{k-1}$ and $\boldsymbol{\mathcal{I}}_{k-1}^k$ denote the grid transfer operators, $\boldsymbol{\mathcal{I}}_k^{k-1} : \mathcal{V}_k \longrightarrow \mathcal{V}_{k-1}$ and $\boldsymbol{\mathcal{I}}_{k-1}^k : \mathcal{V}_{k-1} \longrightarrow \mathcal{V}_k$. The parameters $\nu_1, \nu_2 \geq 0$ denote the number of pre- and post-smoothing steps, respectively.

The k^{th} level iteration $MG(k, \delta\mathcal{U}_0, \mathcal{R})$ of the multigrid algorithm with initial guess $\delta\mathcal{U}_0$ yields an approximation to $\delta\mathcal{U}_k$, the solution of

$$\mathcal{J}_k\delta\mathcal{U} = \mathcal{R} \tag{25}$$

One step can be described concisely throughout two-level Algorithm in Figure 2.

The smoothing in two-grid Algorithm (Figure 2) is performed using Local Pressure Schur complement (LPSC) schemes.

To set the local sub-problems, we introduce prolongation matrices $\boldsymbol{\mathcal{P}}_K^{\tilde{\boldsymbol{u}}}, \boldsymbol{\mathcal{P}}_K^p$, and $\boldsymbol{\mathcal{P}}_K$ defined on spaces of variables values $\mathcal{W}_K := \mathbb{R}^{\dim\mathbb{W}_K}$, $\mathcal{Q}_K := \mathbb{R}^{\dim\mathbb{Q}_K}$, and $\mathcal{V}_K := \mathcal{W}_K \times \mathcal{Q}_K$, respectively. Then, the block Gauss-Seidel iteration reads

$$\mathcal{U}^{l+1} = \mathcal{U}^l - \omega_l \sum_{K \in \mathcal{T}_h} \boldsymbol{\mathcal{P}}_K \left(\boldsymbol{\mathcal{P}}_K^{\mathrm{T}}\left(\frac{\partial\mathcal{R}(\mathcal{U}^l)}{\partial\mathcal{U}}\right)\boldsymbol{\mathcal{P}}_K\right)^{-1} \boldsymbol{\mathcal{P}}_K^{\mathrm{T}}\mathcal{R}(\mathcal{U}^l), \tag{26}$$

RIGHTSLINK

16177061, 2023, 2, Downloaded from https://onlinelibrary.wiley.com/doi/10.1002/pamm.202300062 by Technische Universitaet Dortmund Dezernat Finanzen und Beschaffung, Wiley Online Library on [24/10/2024]. See the Terms and Conditions (https://onlinelibrary.wiley.com/terms-and-conditions) on Wiley Online Library for rules of use; OA articles are governed by the applicable Creative Commons License

TABLE 1

$k\backslash L$	5	6	7	5	6	7	5	6	7
	$\tau_\infty = 0.5$			$\tau_\infty = 1.0$			$\tau_\infty = 2.0$		
5×10^1	4/2	4/2	4/2	3/2	3/3	7/1	3/2	3/3	8/1
1×10^2	4/1	4/2	5/1	4/1	4/2	7/1	4/2	4/2	8/1
5×10^2	4/1	4/1	5/1	3/1	4/1	6/1	4/2	4/2	8/1
1×10^3	4/1	4/1	4/1	4/2	4/2	8/1	4/4	6/1	7/1
5×10^3	4/1	4/1	3/2	7/1	9/1	5/1	6/1	9/1	8/1
1×10^4	4/1	4/2	4/2	5/1	7/1	4/1	7/1	10/1	8/2
	$\tau_\infty = 5.0$			$\tau_\infty = 10.0$			$\tau_\infty = 20.0$		
5×10^1	4/2	3/2	11/1	11/1	4/2	7/1	12/1	5/3	9/1
1×10^2	4/2	5/2	11/1	10/1	5/3	8/1	12/1	6/3	10/1
5×10^2	5/2	4/2	10/1	9/1	5/3	5/1	8/1	5/5	11/1
1×10^3	5/2	9/1	10/1	10/1	9/1	7/1	8/2	9/1	9/2
5×10^3	5/1	5/1	5/1	8/1	8/2	6/1	8/1	7/1	11/1
1×10^4	5/1	5/2	5/1	8/3	7/1	5/1	8/2	7/1	9/1

where $\boldsymbol{\mathcal{P}}_K^{\mathrm{T}}$ denotes the corresponding restriction operator of $\boldsymbol{\mathcal{P}}_K$. In practice, we calculate the local residuum and local matrices as follows

Local residuum:
$$\mathcal{R}_K(\mathcal{U}^l) = \boldsymbol{\mathcal{P}}_K^{\mathrm{T}} \mathcal{R}(\mathcal{U}^l), \tag{27}$$

Local matrices:
$$\left(\frac{\partial \mathcal{R}(\mathcal{U}^l)}{\partial \mathcal{U}}\right)_K = \boldsymbol{\mathcal{P}}_K^{\mathrm{T}} \left(\frac{\partial \mathcal{R}(\mathcal{U}^l)}{\partial \mathcal{U}}\right) \boldsymbol{\mathcal{P}}_K. \tag{28}$$

Then, we solve the local subproblems

$$\left(\frac{\partial \mathcal{R}(\mathcal{U}^l)}{\partial \mathcal{U}}\right)_K \delta \mathcal{U}_K^l = \mathcal{R}_K(\mathcal{U}^l), \tag{29}$$

to get the local update $\delta \mathcal{U}_K^l$. Followed by the calculation of the global update

$$\delta \mathcal{U}^l = \sum_{K \in \mathcal{T}_h} \boldsymbol{\mathcal{P}}_K \delta \mathcal{U}_K^l, \tag{30}$$

and, finally we update the solutions with certain damping parameter ω_l

$$\mathcal{U}^{l+1} = \mathcal{U}^l - \omega_l \delta \mathcal{U}^l. \tag{31}$$

The performance of the solver is investigated throughout thixoviscoplastic lid-driven cavity flow.

4 | NUMERICAL SIMULATIONS

We analyze the performance of the solver for thixoviscoplastic lid-driven cavity flow. We present the statistic of the solver results, that is the number of nonlinear sweeps per average number of linear multigrid sweeps (N/M), for successive mesh level refinement (L). We content to vary the nonlinearity of the problem with respect to thixotropic yield stress τ_∞, and the regularization parameter k. The results are collected blockwise in Table 1 with respect to thixotropic yield stress τ_∞. Furthermore, we plot the unyielded regions with respect to each thixotropic yield stress τ_∞ value on the stream function contours in Figure 3. The nonlinearity of the problem is increased with respect to the increase of the thixotropic yield stress parameter, as it is clearly reflected in Figure 3. On one hand, the unyielded regions spread over the simulation domain. On the other hand, the lip of main vortex move towards the lid and decreases in intensity. Thus, the simulation domain

RIGHTSLINK

16177061, 2023, 2, Downloaded from https://onlinelibrary.wiley.com/doi/10.1002/pamm.202300062 by Technische Universitaet Dortmund Dezernat Finanzen und Beschaffung, Wiley Online Library on [24/10/2024]. See the Terms and Conditions (https://onlinelibrary.wiley.com/terms-and-conditions) on Wiley Online Library for rules of use; OA articles are governed by the applicable Creative Commons License

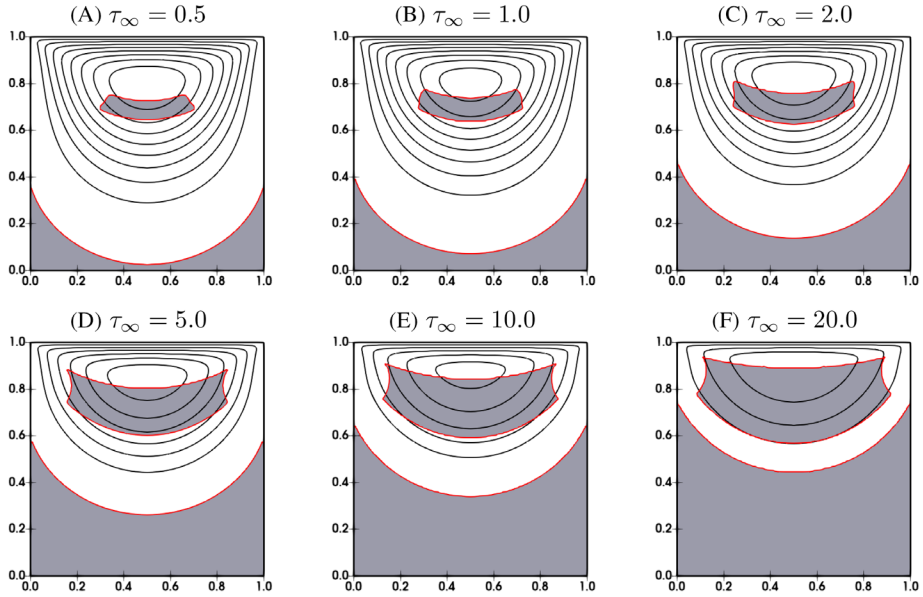

FIGURE 3 Thixoviscoplastic lid-driven cavity flow: the relative position of the unyielded and yielded zones to stream function contours for an increased thixotropic yield stress parameter τ_∞, and $\eta_0 = 1.0$, $\eta_\infty = 0.0$, $\tau_0 = 1.0$, $k = 10^4$, $\mathcal{M}_a = 1.0$, and $\mathcal{M}_b = 0.1$ at level 7.

is dominated by the plastic nonlinearity. Once again this is confirmed by the increase of the number of nonlinear sweeps in Table 1. Furthermore, the nonlinearity of the problem is increased with respect to the increase of the regularization parameter, which can not be clearly seen in terms of the increase of nonlinear sweeps as we are using the continuation process for the starting solutions for the nonlinear solver with respect to regularization parameter. That is, the solutions of smaller regularization parameter are used as a starting solutions for higher regularization parameter. Most importantly, the nonlinearity of the problem is similar for each refinement level, which enables a proper analysis of the corresponding linear solver. And the most striking point is the linear solver efficiency, that is the mesh refinement independent behavior of multigrid.

5 | SUMMARY

We presented Newton-multigrid FEM solver for thixoviscoplastic flow problems. As an example of mutifield nonlinear coupled problems, thixoviscoplastic flow presents numerical challenges with respect to nonlinearity as well as the coupling. Thus, the importance of the optimal choice of FEM techniques and algorithmic tools to delicately handle the problem's nonlinearity and coupling. We based our investigation on the wellposedness and error analysis results of thixoviscoplastic flow problems published in *Proc. Appl. Math. Mech.* [1, 2] to develop a Newton-multigrid solver. We used LPSC concept to solve the coupled problem on mesh's elements, and proceed with outer block Gauss-Seidel iteration to update the global solutions. Two important consequences of using the well established FEM analysis on FEM discretization are as follows. Firstly, the choice of linear *discontinuous* pressure results in optimal choices of the Gauss-Seidel's blocks. Secondly, the same quadratic interpolation choice for velocity and microstructure results in an efficient treatment of velocity-microstructure coupling due to noncoupling of microstructure and pressure. Furthermore, we used combined adaptive discrete Newton's method and geometric multigrid to obtain the approximate solutions. The adaptivity idea for the discrete Newton's method is based on Jacobian calculations, using both the actual convergence rate of nonlinear problem and the step-length control in discrete differencing operation. Meanwhile, the linear multigrid solver is made to meet optimally the nonlinear solver convergence requirement. The resulting solver is black box controlled only with the actual rate of convergence. The efficiency of the solver is tested on well-known lid-driven cavity configuration upgraded for thixoviscoplastic flow. We investigated the performance of the solver on mesh level refinement for two different nonlinearity control model parameters, thixotropic yield stress and regularization. The efficiency of the solver is strongly expressed via the mesh refinement independent behavior for both model parameters.

16177061, 2023, 2, Downloaded from https://onlinelibrary.wiley.com/doi/10.1002/pamm.202300062 by Technische Universitaet Dortmund Dezernat Finanzen und Beschaffung, Wiley Online Library on [24/10/2024]. See the Terms and Conditions (https://onlinelibrary.wiley.com/terms-and-conditions) on Wiley Online Library for rules of use; OA articles are governed by the applicable Creative Commons License

RIGHTSLINK

ACKNOWLEDGMENTS

The authors acknowledge the funding provided by the "Deutsche Forschungsgemeinschaft (DFG, German Research Foundation) - 446888252". We would also like to gratefully acknowledge the support by LSIII and LiDO3 team at ITMC, TU Dortmund University, Germany.

ORCID

Naheed Begum https://orcid.org/0000-0001-7707-572X

REFERENCES

1. Begum, N., Ouazzi, A., & Turek, S. (2023). FEM simulation of thixo–viscoplastic flow problems: Error analysis. *Special Issue: 92nd Annual Meeting of the International Association of Applied Mathematics and Mechanics (GAMM)*, *23*(1), e202200294. https://doi.org/10.1002/pamm.202200294
2. Begum, N., Ouazzi, A., & Turek, S. (2021). Monolithic Newton-multigrid FEM for the simulation of thixotropic flow problems. *Proceedings in Applied Mathematics and Mechanics*, *21*, e202100019. https://doi.org/10.1002/pamm.202100019
3. Houška, M. (1981). *Engineering aspects of the rheology of thixotropic liquids* [PhD Thesis]. Faculty of Mechanical Engineering, Czech Technical University of Prague.
4. Girault, V., & Raviart, P. A. (1979). *Finite Element Approximation of the Navier Stokes Equations*. Lecture Notes in Mathematics, Vol. 749. Springer.
5. Fatima, A., Turek, S., Ouazzi, A., & Afaq, A. (2021). An adaptive discrete newton method for regularization-free Bingham model. *Ergebnisberichte des Instituts für Angewandte Mathematik Nummer 635, Fakultät für Mathematik*, TU Dortmund University, 635.
6. Mehlmann, C., & Richter, T. (2017). A modified global Newton solver for viscous-plastic sea ice models. *Ocean Modelling*, *166*, 96–107. https://doi.org/10.1016/j.ocemod.2017.06.001
7. Worrall, W. E., & Tuliani, S. (1964). Viscosity changes during the aging of clay-water suspensions. *Transactions of the British Ceramic Society*, *63*, 167–185.
8. Coussot, P., Nguyen, Q. D., Huynh, H. T., & Bonn, D. (2002). Viscosity bifurcation in thixotropic, yielding fluids. *Journal of Rheology*, *46*(3), 573–589.
9. Mujumdar, A., Beris, A. N., & Metzner, A. B. (2002). Transient phenomena in thixotropic systems. *Journal of Non-Newtonian Fluid Mechanics*, *102*(2), 157–178.

How to cite this article: Begum, N., Ouazzi, A., & Turek, S. (2023). Efficient Newton-multigrid FEM solver for multifield nonlinear coupled problems applied to thixoviscoplastic flows. *Proceedings in Applied Mathematics and Mechanics*, *23,* e202300062. https://doi.org/10.1002/pamm.202300062

APPENDIX

Thixotropic models are results of two-field, velocity and microstructure, interplay via thixotropic plastic viscosity, thixotropic yield stress, breakdown, and buildup functions. In the following Table A1, we collect examples of thixotropic models.

TABLE A1 Thixotropic models.

	η	τ	$\mathcal{F}$	$\mathcal{G}$
Worrall et al. [7]	$\lambda\,\eta_0$	τ_0	$\mathcal{M}_a(1-\lambda)\|\mathbf{D}\|$	$\mathcal{M}_b\lambda\|\mathbf{D}\|$
Coussot et al.[8]	$\lambda^g\,\eta_0$		$\mathcal{M}_a$	$\mathcal{M}_b\lambda\|\mathbf{D}\|$
Houška [3]	$(\eta_0+\eta_\infty\lambda)\|\mathbf{D}\|^{n-1}$	$(\tau_0+\tau_\infty\lambda)$	$\mathcal{M}_a(1-\lambda)$	$\mathcal{M}_b\lambda^m\|\mathbf{D}\|$
Mujumbar et al. [9]	$(\eta_0+\eta_\infty\lambda)\|\mathbf{D}\|^{n-1}$	$\lambda^{g+1}G_0\Lambda_c$	$\mathcal{M}_a(1-\lambda)$	$\mathcal{M}_b\lambda\|\mathbf{D}\|$

Here η_0 and τ_0 are initial plastic viscosity and yield stress, respectively. η_∞ and τ_∞ are thixotropic plastic viscosity and yield stress. Λ_c , and G_0 are elastic parameters, $\mathcal{M}_a$ and $\mathcal{M}_b$ are buildup and breakage constants, and g, p, m, n are rate indices.

RIGHTSLINK

16177061, 2023, 2, Downloaded from https://onlinelibrary.wiley.com/doi/10.1002/pamm.202300062 by Technische Universitaet Dortmund Dezernat Finanzen und Beschaffung, Wiley Online Library on [24/10/2024]. See the Terms and Conditions (https://onlinelibrary.wiley.com/terms-and-conditions) on Wiley Online Library for rules of use; OA articles are governed by the applicable Creative Commons License